

## Coloring a Lorentz gas

Steve Nielsen and Raymond Kapral<sup>a)</sup>

*Chemical Physics Theory Group, Department of Chemistry, University of Toronto, Toronto, Ontario M5S 3H6, Canada*

(Received 18 May 1998; accepted 15 July 1998)

A catalytic site is introduced into a two-dimensional Lorentz gas system consisting of three disks arranged in an equilateral triangle to model reactive dynamics. This system is studied at a microscopic level using an  $N$ -cylinder description where the exact dynamics is replaced by a symbolic dynamics which is a generating partition. The Kolmogorov–Sinai entropy and its finite and colored varieties are discussed. These are then related to the colored escape rate, a macroscopic property. Lastly, escape is eliminated by extending the three disk system to an infinite lattice, and the color correlation function is studied. For large catalytic regions the Poisson process rate law expression breaks down. © 1998 American Institute of Physics. [S0021-9606(98)50739-8]

### I. INTRODUCTION

The derivation of kinetic equations for chemically reacting systems is a fundamental problem of statistical mechanics. Most approaches involve phenomenological elements, and remain poorly justified from first principles. Since the underlying equations of classical mechanics are deterministic and time-reversal symmetric, questions associated with the irreversibility of macroscopic chemical rate equations must be addressed.

The typical assumption made in most molecular-dynamics investigations of reaction dynamics is that the many-body system is chaotic and the chaotic dynamics provides the basis for a statistical description. Since the chaotic properties of many-body systems are difficult to establish, it is interesting to consider low-dimensional systems where detailed studies can be made.

There have been several investigations of simple, low-dimensional, deterministic dynamical systems which attempt to provide insight into the microscopic origin of macroscopic chemical rate laws. DeLeon and Berne<sup>1</sup> have constructed a simple model of a chemical interconversion process where the phase space of each chemical species is a stadium billiard, a system known to have strongly mixing properties (K system). Reaction occurs when the particle passes from one stadium to the other through a small hole. In a similar spirit, a chemical interconversion process was modeled by transfer between phase space domains whose dynamics was governed by baker's transformations,<sup>2</sup> a dynamical system that is also known to have strongly mixing properties (Bernoulli). Spatially extended generalizations of this model have recently been studied by Gaspard and Klages.<sup>3</sup> Even simpler, ideal-gas-type models have been studied where particles travel in straight-line paths.<sup>4</sup> Particles are assigned colors and when two trajectories cross a color change (reaction) occurs. All of these studies have attempted to link the reaction dynamics to the mixing properties of the underlying determin-

istic dynamics and establish the conditions under which rate laws apply.

Another system that has received considerable attention is the Lorentz gas,<sup>5–14</sup> which consists of a particle which moves freely between elastic collisions with fixed hard disk scatterers. It is known that this system is chaotic; it has a positive Lyapunov exponent and a positive Kolmogorov–Sinai entropy. Lorentz gas systems comprising three disks, as well as an infinite array of disks, were studied by Gaspard and Rice<sup>5</sup> and Gaspard and Nicolis.<sup>6</sup> The escape rate of particles from the system (or a sub-domain of the system) was studied and related to dynamical systems properties such as the Kolmogorov–Sinai entropy and the Lyapunov exponents.

In this paper we also study Lorentz gas systems consisting of three disks arranged in an equilateral triangle (Fig. 1) or infinite arrays of such disks. However, we suppose that two species of particles exist in the system and collide with the disks. A portion (or portions) of a disk perimeter is assumed to be a catalytic site such that if a particle strikes the catalytic site a reaction occurs and it converts to the other species. It is convenient to denote the two chemical species by the color labels “black” and “white” and the reaction as a color changing process. These reactive and nonreactive collision events are depicted in Fig. 1, which also shows particles leaving the system; we consider a particle to escape the system when it crosses one of the straight boundary lines. Hence, black and white particles interconvert and escape.

The particle's speed is chosen to be unity. An ensemble of (noninteracting) particles is used to calculate statistical quantities. One might expect that the chaotic nature of the system will lead to a simple exponential law for the late-time decay of species populations due to reaction and escape. In this late-time domain a phenomenological picture

$$\text{escape} \xleftarrow[k]{k_B} \mathcal{B} \xrightleftharpoons[k]{k} \mathcal{W} \xrightarrow{k_W} \text{escape}, \quad (1)$$

should be appropriate.

This is certainly a highly schematic version of a reacting system; however, it captures some of the essential elements

<sup>a)</sup>Electronic mail: rkapral@gatto.chem.utoronto.ca

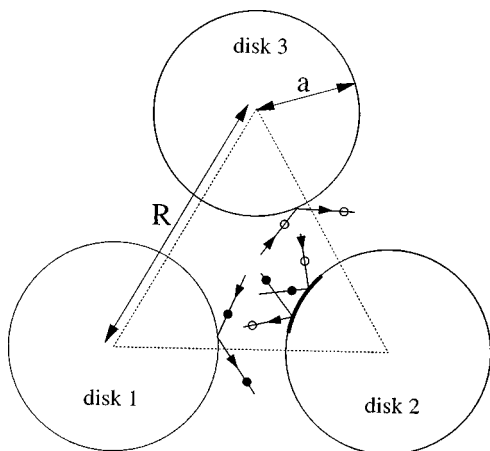


FIG. 1. Colored Lorentz system. Two particles are shown escaping the system and two particles are shown changing color by striking a catalytic site, shown in heavy line.

of reactions involving small molecules in a porous medium containing active sites that promote reaction, or even surface reactions involving the dynamics of small molecules that react at specific sites. Of course, our purpose is not to attempt to model such real systems but rather the focus of this study is to probe the origin and possible breakdown of phenomenological pictures and to provide links between microscopic and macroscopic quantities.

The outline of the paper is as follows. In Sec. II the uncolored system is studied and a symbolic dynamics is introduced. The repeller is considered and the  $N$ -cylinders and Kolmogorov–Sinai entropy are defined. Section III presents the phenomenological picture of Eq. (1) and then focuses on the early-time behavior of the system. In Sec. IV the escape rate constants of the phenomenological picture are shown to be distinct and to vary with the location of the catalytic site. These colored escape rates are connected to both the repeller and to a colored extension of the Kolmogorov–Sinai entropy. Our results indicate that Pesin’s theorem cannot be simply extended to the reactive case as defined in this study.

In Sec. V the second example of a reactive Lorentz gas, a periodic arrangement of disks with catalytic sites on a triangular lattice, is studied. A particle introduced into the system now moves from one three-disk domain to another instead of escaping from the system. This allows us to study the breakdown of the phenomenological rate law, which occurs when the catalytic domain is large. Concluding remarks are made in Sec. VI.

## II. UNCOLORED SYSTEM

In order to define the quantities used and generalized in the subsequent analysis, we begin with a few remarks on the dynamics of the uncolored three-disk problem. The numerical results presented here and in the rest of the paper take  $R=3.11a$  (cf. Fig. 1). This configuration is generic for the class of systems ( $R>3a$ ) in which a particle starting on the boundary of disk one (within the allowed domain) can reach any point on the boundaries of disks two and three (again within the allowed domain) directly.

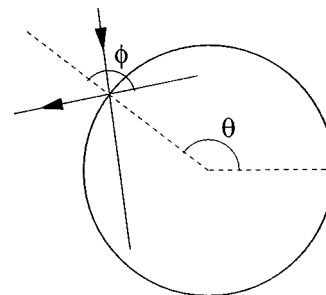


FIG. 2. Definition of  $\theta$  and  $\phi$ . The angle  $\phi$  is measured from the outgoing trajectory to the normal. The angle  $\theta$  locates the point of impact on the disk.

### A. Repeller

Due to the convex walls of the disks, the dynamics is everywhere defocusing so that there are no stable orbits. Yet some trajectories survive under the dynamics; the set of these form a fractal object called a repeller. Trajectories starting on the repeller will never leave it. This defines a probability distribution: The natural invariant probability distribution on a repeller tells us how often the various parts of the repeller are visited by trajectories that never escape. Trajectories coming close to the repeller are responsible for the phenomenon of transient chaos—chaotic behavior that takes place for a long but finite time.

### B. Definition of $\theta$ and $\phi$

In order to study the trajectories systematically, we focus solely on the collision events, since the trajectories follow straight line paths in between. Two variables are needed to describe a collision: The position and velocity of the trajectory upon impact. We choose (following Gaspard and Rice<sup>5</sup>)  $\theta$  and  $\phi$  as shown in Fig. 2.

### C. Symbolic dynamics, $N$ -cylinders, and a generating partition

A symbolic dynamics is associated with trajectories by sequentially recording the numbers of the disks which are struck. We let  $i_n$  ( $i_n \in \{1,2,3\}$ ) be the number of the disk which is struck on the  $n$ th collision. A given symbol sequence of finite length  $N$  encompasses many different trajectories because each symbol corresponds to a finite volume of phase space. We say the symbolic dynamics is a generating partition if the infinite symbol sequence  $i_1, i_2, \dots, i_n, \dots$  uniquely determines the initial condition  $\zeta_1 = (\theta_1, \phi_1)$ .<sup>15</sup> This is satisfied for our system if we ignore the particle’s path until it first hits a disk and call this the (new) initial condition  $\zeta_1$ . To obtain an infinite symbol sequence, the corresponding trajectory must remain in the system forever; it must be trapped and hence a member of the repeller. We define the  $N$ -cylinder  $i_1 i_2 \dots i_N$  to be the set of all trajectories which hit disk  $i_1$  on their first collision, disk  $i_2$  on their second collision,  $\dots$ , disk  $i_N$  on their  $N$ th collision, and then either undergo further collisions or escape the system. Each individual  $N$ -cylinder has contributions in two or three of the disk phase spaces, and there are  $3 \cdot 2^{N-1}$  total  $N$ -cylinders.

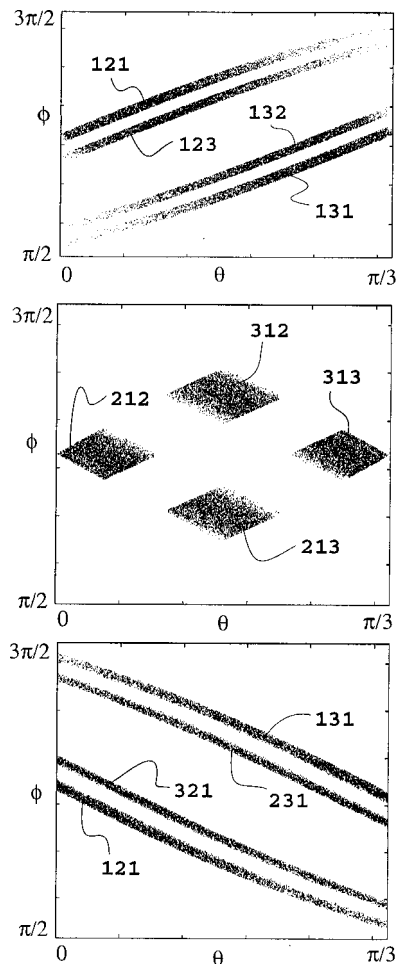


FIG. 3. Starting from an ensemble of trajectories with uniform random initial conditions, a graphical representation of the three-cylinders is obtained from the subensemble of trajectories which strike at least three disks. From these trajectories, the  $\theta$ - $\phi$  phase space coordinates of the first, second, and third collisions with disks are plotted in the top, middle, and bottom panels, respectively (disk one phase space only). See text for details.

For example, the three-cylinders can be visualized as follows. Each constituent trajectory of the three-cylinders strikes at least three disks. For each of these first three hits, we plot the trajectories in the  $\theta$ - $\phi$  variables of the disk being struck (Fig. 3). Only the phase space corresponding to disk one is shown because the pattern is identical for the other disks (by symmetry). Note that two of the three-cylinders, 121 and 131, appear twice. This is because trajectories belonging to these three-cylinders strike disk 1 on their first and third hits, and hence, they appear twice because we are grouping trajectories by hit number.

In the first three panels of Fig. 4 we simplify this visualization slightly by plotting histograms of the data in Fig. 3. A very narrow bin width is used so that the functions shown in Fig. 4 represent the relative frequency of collisions as a function of  $\theta$ . Denoting these functions  $\rho_1(\theta)$ ,  $\rho_2(\theta)$ , and  $\rho_3(\theta)$ , the overall collision frequency of the three-cylinders is given by  $\rho(\theta) = \frac{1}{3} \sum_{n=1}^3 \rho_n(\theta)$ , shown in the lower right panel of Fig. 4.

Each hit number has its own measure over the disks, and these follow a recursive pattern which in the limit  $N \rightarrow \infty$ , yields the fractal pattern which is the collision frequency

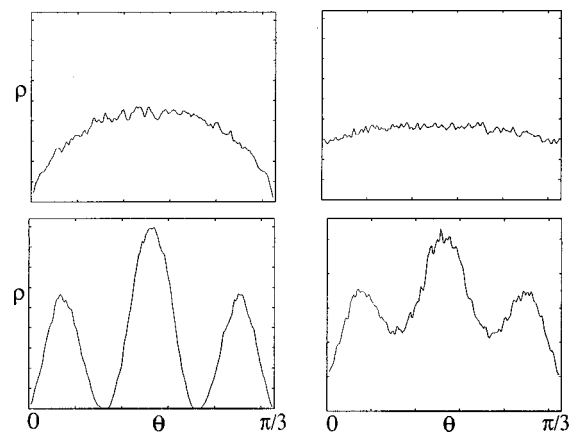


FIG. 4. The collision frequency functions  $\rho_n(\theta)$  of the three-cylinders. Shown are the functions for hit one (upper left), hit two (lower left), and hit three (upper right). The lower right panel shows the net collision frequency function of all three hits. See text for details. The frequency is expressed in arbitrary units.

(probability density) of the repeller. The  $N=9$  collision frequency function  $\rho(\theta) = \frac{1}{9} \sum_{n=1}^9 \rho_n(\theta)$  is shown in Fig. 5; comparing this to the lower right panel of Fig. 4 indicates how the refinement proceeds. At each level  $N$  of the hit-number pattern, hit numbers  $i$  and  $N+1-i$  are similar. This is due to time-reversal symmetry. Two factors affect the exact relationship. Firstly,  $\phi$  is measured from the outgoing trajectory to the normal, and since reversing time changes incoming trajectories into outgoing trajectories we must use the relation  $\phi^{\text{out}} + \phi^{\text{in}} = 2\pi$  to account for this change of reference. Secondly, the relation is affected by the choice of initial conditions. We notice that the hit-number-three collision frequency function for the three-cylinders (upper right panel of Fig. 4) has a flatter distribution than the corresponding function for hit number one (upper left panel of Fig. 4). The function for hit one is a consequence of the initial conditions, which are uniform and random inside the three-disk domain. The resulting first-collision frequency profile as a function of  $\theta$  is low at  $\theta=0, \pi/3$  and high at  $\theta=\pi/6$ . This is because of the proximity of the extreme values of  $\theta$  to the exit channels, from which no trajectories emanate. The dynamics is defocusing, hence it is not surprising that the distribution at hit three is flatter.

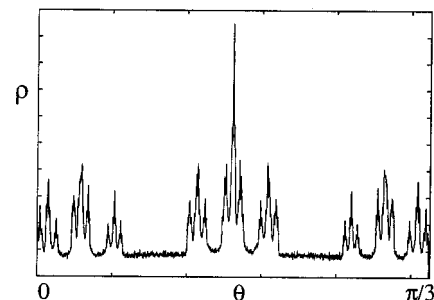


FIG. 5. The level  $N=9$  approximation to the probability density of the repeller, showing the collision frequency function  $\rho(\theta)$  of the nine-cylinders (see the lower right panel of Fig. 4 for comparison and the text for details). Arbitrary units; phase space shown for disk one only by symmetry.

TABLE I. Uncolored  $h_{KS}^N$ .

$N$	$h_{KS}^N$	Maximum [Eq. (5)]
3	0.828	0.8283
5	0.772	0.7742
7	0.748	0.7511
9	0.733±0.002	0.7382
11	0.721±0.01	0.7300

### D. Kolmogorov–Sinai entropy $h_{KS}$

The probability of observing a given  $N$ -cylinder  $N_i$  is denoted by  $p(i_1, \dots, i_N)$ . It depends on  $\sigma$ , the measure of initial conditions. The Kolmogorov-Sinai entropy is defined as

$$h_{KS} = - \sup_{\{P\}} \lim_{N \rightarrow \infty} \frac{1}{N} \times \sum_{i_1, \dots, i_N} p(i_1, \dots, i_N) \ln p(i_1, \dots, i_N), \quad (2)$$

where a supremum is taken over all partitions of the phase space and  $\sigma$  is taken to be  $\mu$ , the natural invariant measure of the repeller. The generating partition  $\mathcal{G}$  introduced above achieves this supremum.<sup>15</sup> Thus

$$h_{KS} = - \lim_{N \rightarrow \infty} \frac{1}{N} \times \sum_{i_1, \dots, i_N} p(i_1, \dots, i_N) \ln p(i_1, \dots, i_N). \quad (3)$$

Furthermore, at level  $N$ , the logical approximation to  $\mu$  is the probability distribution associated with the  $N$ -cylinders; i.e., the level- $N$  coarse-grained distribution.

A chaotic system can be defined as one for which  $h_{KS} > 0$ . This quantity gives the data-accumulation rate necessary to follow the time evolution and to recover the trajectory of the system from the recorded data.<sup>6</sup> If every  $N$ -cylinder has equal probability, then

$$p(i_1, \dots, i_N) = (3 \cdot 2^{N-1})^{-1}, \quad (4)$$

so that at level  $N$

$$h_{KS}^N = - \frac{1}{N} \ln((3 \cdot 2^{N-1})^{-1}) = \ln 2 + \frac{\ln 3 - \ln 2}{N}. \quad (5)$$

For our system Eq. (5) holds approximately, but only low  $N$  values are feasible computationally (Table I).

### III. PHENOMENOLOGICAL & EARLY-TIME BEHAVIOR

We now consider the reactive dynamics when a catalytic site is introduced on the surface of disk one. As described in the Introduction, the catalytic site causes interconversion of black and white species which may then escape from the three-disk domain. We restrict our considerations to the specific initial color condition of all white particles in order for the color label to serve its purpose most effectively; this

purpose is to draw attention to particular classes of trajectories, such as those which leave the system after reacting.

#### A. Phenomenological picture

If a phenomenological description in terms of a mass-action rate law derived from the mechanism in Eq. (1) is adopted, the evolution equation for the number of black and white particles as a function of time ( $\bar{n}_B(t), \bar{n}_W(t)$ ) is

$$\frac{d\bar{n}_B}{dt} = -k\bar{n}_B + k\bar{n}_W - k_B\bar{n}_B, \quad (6)$$

where a similar equation for  $\bar{n}_W(t)$  may be written by the relabeling  $B \leftrightarrow W$ . Given the all-white-particle initial condition

$$\bar{n}_B(0) = 0, \quad \bar{n}_W(0) = 1, \quad (7)$$

the black-density evolution is

$$\bar{n}_B(t) = \left[ \frac{k}{\sqrt{4k^2 + (k_W - k_B)^2}} \right] [e^{\lambda_- t} - e^{\lambda_+ t}] \quad (8)$$

with

$$\lambda_{\pm} = -\frac{1}{2} \{ 2k + k_W + k_B \pm \sqrt{4k^2 + (k_W - k_B)^2} \}. \quad (9)$$

The asymptotic slope  $\lambda_-$  includes all three rate constants of Eq. (1).

A phenomenological picture of this type is expected to be applicable only on long-time scales and under circumstances where the microscopic details of the collision dynamics are not observable. For instance, with an all-white-particle initial condition, a white particle must first strike a catalytic site and react to form a black particle to contribute to  $\bar{n}_B(t)$ . The phenomenological model predicts black particle escape on arbitrarily short time scales. We now examine some of the features of the reaction dynamics and escape processes.

#### B. Initial events

The initial rate at which white particles react to form black particles is easily computed. Consider a uniform initial velocity and position distribution of white particles. The catalytic site is immediately subjected to a constant flux of white particles, and hence the initial production of black particles occurs at a constant rate. This rate is evaluated as follows.

The circumference of a disk is partitioned into  $n$  equal pieces, so that each is subtended by an arc  $\theta = 2\pi/n$  (Fig. 6). For each piece the circumference is approximated by a straight line tangent to the disk at the midpoint. The length of this line segment is  $2a \tan(\pi/n)$  which we approximate as  $2\pi a/n$ . We wish to look at trajectories hitting the line segment within time  $\Delta t$ . Fixing the velocity to a specific direction  $\phi$ , the allowed position space is given by a parallelogram of area (shaded area in Fig. 6)

$$A = \frac{2\pi a}{n} \Delta t \sin \phi. \quad (10)$$

Hence the total phase space contribution is

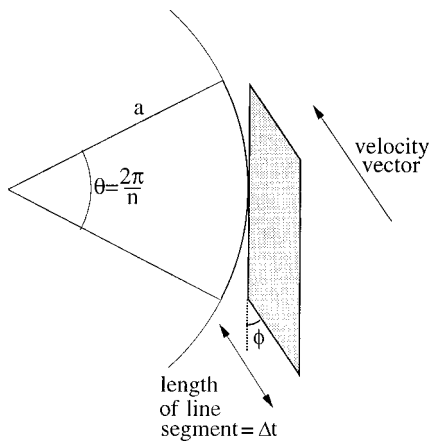


FIG. 6. Calculation of initial rate.

$$2 \int_0^{\pi/2} \frac{\pi/2 \pi a}{n} \Delta t \sin \phi d\phi = \frac{4 \pi a \Delta t}{n}. \quad (11)$$

Taking the Riemann limit yields, for the entire disk

$$\sum_{i=1}^n \frac{4 \pi a \Delta t}{n} = 4 \pi a \Delta t. \quad (12)$$

This result is valid for any time  $\Delta t$ . It also allows the area of interest to be a catalytic site instead of the entire disk. For a catalytic site subtended over an angle of  $\phi$  the volume of phase space hitting this site within time  $\Delta t$  is  $2 \phi a \Delta t$ , giving a constant rate of

$$k_i = 2 \phi a. \quad (13)$$

### C. Early-time behavior

Next, we describe the early-time evolution of the system. In the set of snapshots shown in Fig. 7, the catalytic site is centered at  $\theta = \pi/6$  on disk one and spans a total angle of 0.04 radians. As time increases from zero white particles strike the catalytic site, turning black and bouncing outwards from this region. At  $t = 1.00$ , black particles have propagated to the boundary and are escaping the system. At  $t = 1.50$  some of the black particles have struck disks two and three. At  $t = 2.00$  the fronts propagating from disks two and three have almost met; parts of these fronts are visible in the white gap region close to disk one seen at  $t = 1.50$ . Most striking is the appearance of a hole at  $t = 2.00$  close to the colored region. By now all direct collisions with the colored region have occurred—all particles striking the colored region must have first struck disk two or disk three. This constrains the velocity vectors of the newly colored black particles. At  $t = 2.60$  this hole has grown, and the black particles rebounding from disks two and three have reached disk one, so that a few of the black particles can now change color. The hole has opened completely at  $t = 3.50$ . The loss of all discernible structure at  $t = 10.00$  is worth noting.

These dynamical features are reflected in the structure of the fraction of black particles  $\bar{n}_B(t)$  in the system at time  $t$ . This fraction is plotted in Fig. 8 for two locations of the

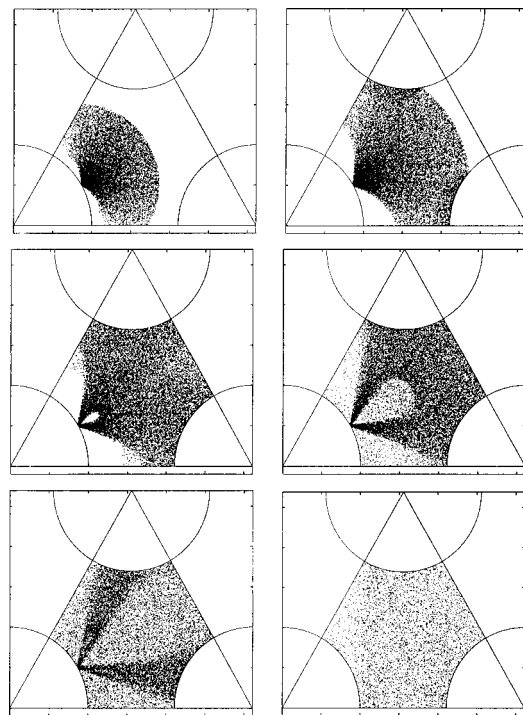


FIG. 7. The catalytic site spans  $\theta \in [\pi/6 \pm 0.02]$  on disk one. Reading left to right, top to bottom, snapshots of the black particle density are shown at times of  $t = 1.00, 1.50, 2.00, 2.60, 3.50, 10.00$ .

catalytic site: centered on  $\theta = \pi/6$  as described above (upper curve) and centered on  $\theta = 0.02$  near the edge of the disk one boundary.

The derivation in Sec. III B predicts an initial rate (with a catalytic site of angle 0.04 radians and  $a = 1$ ) of  $k_i = 0.08$ . This value agrees with the upper curve of Fig. 8 as expected, while the curve for the second choice of catalytic site location bends away from this initial rate immediately. This difference is due to the fact that in the upper curve there is an initial buildup of black density with no escape, whereas for the second choice black particles escape immediately. Note the dip in  $\bar{n}_B(t)$  for  $\theta = \pi/6$ . This has its origin in the opening up of the “hole” at  $t = 3.5$  as discussed above. These two choices represent the two extremes for the initial behavior of

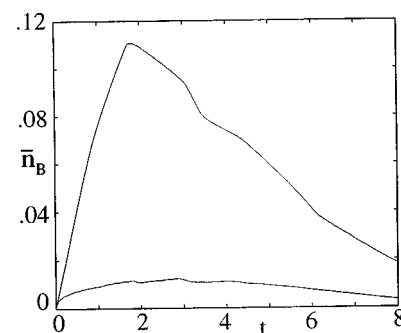


FIG. 8. Fraction of black particles in the system at time  $t$ . The upper curve corresponds to  $\theta = \pi/6$  described in Fig. 7. Note the initial linear behavior. The lower curve corresponds to exactly the same scenario, but with the catalytic site at the edge of the disk one boundary (and still spanning a total angle of 0.04 radians).

the system with a single catalytic site. As noted earlier, in the phenomenological picture escape and reaction occur all of the time at fixed rate, and so this picture does not account for the structured dynamics in the early-time regime.

#### IV. COLORED ESCAPE RATES AND ENTROPIES

In closed systems (with no catalytic sites) the Kolmogorov–Sinai entropy  $h_{KS}$  and the sum of the positive Lyapunov exponents  $\lambda_i$  are related by Pesin’s theorem<sup>15</sup>

$$h_{KS} = \sum_{\lambda_i > 0} \lambda_i. \quad (14)$$

For open systems the escape rate  $\gamma$  is included in a generalization of Eq. (14) as

$$\gamma = \sum_{\lambda_i > 0} \lambda_i - h_{KS}, \quad (15)$$

which has been shown to hold for several classes of systems.<sup>5,6,10,15,16</sup> In particular it holds for our system when no catalytic site is present. Equation (15) has been interpreted as saying that dynamical randomness inhibits escape from the repeller. These relations are important because they link a macroscopic quantity, namely the escape rate, with dynamical-systems quantities, namely the Kolmogorov–Sinai entropy and the Lyapunov exponents.

##### A. Are the two escape rates different?

When a catalytic site is present and one observes the escape of black or white particles, these relations do not generalize in an obvious manner. Two escape rates appear in the phenomenological model and an important question to address is whether these two escape rates  $k_W$  and  $k_B$  are identical or not. To answer this question we eliminate the color changing process as follows.

With an all-white initial condition, some particles will change color an odd number of times and will thus exit colored black. For such trajectories, we pretend that the particle was initially black and never changed color. In this manner we eliminate the (color changing) reaction in favor of changing the initial condition to a mixture of black and white particles, which then merely propagate retaining their color labels. This procedure is implemented by taking trajectories which escape black, changing their color histories to all black, and then storing the resulting data. The result (Fig. 9) clearly shows that the escape rates vary with the initial distribution of particles of each color, and hence that they are distinct from one another in a nontrivial way. It should be noted that the exponential decay starts after  $t \approx 7$  (see Figs. 7 and 8). The white escape rate does not vary noticeably with the location of the (small) coloring region, and remains at the uncolored escape rate value of  $\gamma = 0.866$ .

##### B. Colored Kolmogorov–Sinai entropy

We now construct a colored version of the Kolmogorov–Sinai entropy,  $h_C$ . To do this we modify Eq. (3) by restricting the trajectories which contribute to the probabilities  $p(i_1, \dots, i_N)$  to those which escape colored black (from an all-white initial condition). In other words,

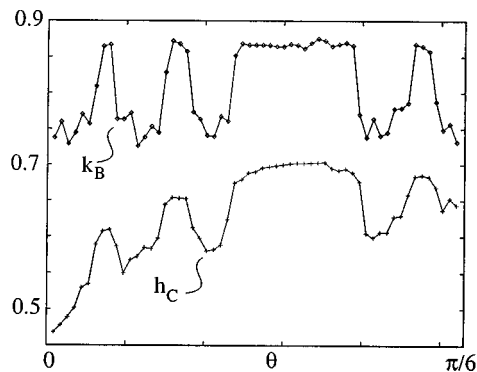


FIG. 9. Black escape rate (diamonds) and the  $N=7$  curve of Fig. 10 (crosses). Each diamond is the slope of the logarithm of the number of black particles in the system as a function of time (ignoring the initial nonexponential behavior). Each diamond represents a catalytic site on disk one centered on the  $\theta$ -location of the diamond and extending one diamond to either side. The escape rate for the uncolored system is  $\gamma = 0.866$ , and this is also the value of the white escape rate  $k_W$  for all the data shown (Ref. 17).

we exclude all trajectories which do not escape black from contributing to the probabilities  $p(i_1, \dots, i_N)$ . Figure 10 shows some finite approximations to the colored entropy for small catalytic sites (see figure caption for details).

Our simulations show that there is a qualitative relationship between the black escape rates, the colored Kolmogorov–Sinai entropies (as shown in Fig. 9), and the invariant density of the repeller. It should be noted that the resolution of the  $h_C$  plot and of the black escape rate plot is very low compared to that of the repeller. The blow-ups in Fig. 10 show that the fine detail is present if the catalytic sites are made small enough.

The three relations shown in Figs. 5, 9, and 10 are summarized as follows:

- (1) Higher density of (uncolored) repeller  $\Leftrightarrow$  lower (colored) escape rate.
- (2) Higher density of (uncolored) repeller  $\Leftrightarrow$  lower (colored, finite) entropy.

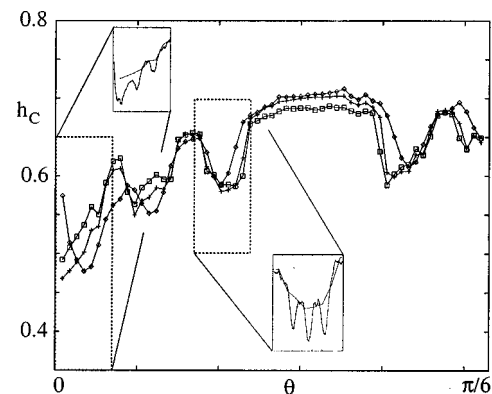


FIG. 10. The colored  $h_C^N$  for  $N=5$  (diamonds),  $N=7$  (crosses), and  $N=9$  (squares). Each symbol is the colored Kolmogorov–Sinai entropy for a catalytic site on disk one centered at the  $\theta$ -location of the symbol and extending one symbol to either side. Only  $\theta = [0, \pi/6]$  is shown because  $\theta = [\pi/6, \pi/3]$  is the reflection of this in the line  $\theta = \pi/6$  (by symmetry). The blow-ups show  $N=7$  at the original resolution and at a finer resolution.

- (3) Lower (colored) escape rate  $\Leftrightarrow$  lower (colored, finite) entropy.

Point one is intuitive; trajectories which sample the high-density regions of the repeller stay in the system longer than trajectories which sample the low-density regions. Point three is a consequence of one and two, so we now focus on point two. Decomposing the  $N$ -cylinders into hit numbers (as in Figs. 3 and 4) allows us to understand point two. For each different hit number the same  $N$ -cylinders are present, albeit in different arrangements. The color changing event is independent of  $\phi$ , so that, for instance, all of the  $N$ -cylinders for hit numbers one and  $N$  are approximately degenerate. As we move in towards the middle hits, the  $N$ -cylinders become less and less degenerate. Let us consider two catalytic sites, one contained in the largest gap of Fig. 5 (e.g.,  $\theta \approx \pi/10$ ) and one contained in the second largest gap of Fig. 5 (e.g.,  $\theta \approx 0.162$ ); the sites are chosen to have the same measure. For the first catalytic site particles which make  $N$  hits before escaping can only change color on their first or last hit. This is because the  $N$ -cylinder density is zero over this catalytic site for all hit numbers except these two. Since the  $N$ -cylinders are approximately degenerate for these two hits, the particles are equally likely to belong to any of the  $N$ -cylinders; this maximizes the colored entropy. For the second coloring choice, there is nonzero  $N$ -cylinder density for the first and last hits, and also for the second and second last hits. Particles changing color on their first or last hits are equally likely to belong to any of the  $N$ -cylinders, so once again all of the  $N$ -cylinders have equal probability associated with them. But particles which change color on their second or second last hits skew this probability distribution to favor the particular  $N$ -cylinders whose density overlaps the coloring region. When the resulting probabilities are normalized and summed [Eq. (3) and Sec. IV B] the entropy decreases relative to the first catalytic site case. This argument can be elaborated and shows that we should expect the colored entropy to decrease when the repeller density increases. This relationship is opposite to that predicted by a simple extension of Pesin's theorem.

## V. INFINITE ARRAY OF CATALYTIC SITES

As a second example of a reactive Lorentz gas, we extend our three disk system to a periodic arrangement of disks on a triangular lattice (Fig. 11). A particle introduced into this system now moves from one three-disk region to another instead of escaping the system. If we introduce catalytic sites in each three-disk domain in the same manner (for example, by placing catalytic sites in pairs  $\pi$  radians apart on every disk), then it is sufficient to consider one three-disk domain with the appropriate boundary conditions (Fig. 11). In this manner we obtain a reactive trajectory of arbitrary length in a single three-disk domain. Note that escape has been eliminated so that the only rate process left is the color changing reaction. The phenomenological picture is

$$\mathcal{B} \xrightleftharpoons[k]{k} \mathcal{W}. \quad (16)$$

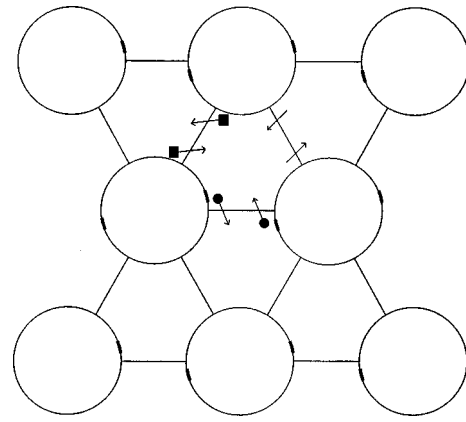


FIG. 11. An infinite array of catalytic sites showing appropriate boundary conditions to revert back to a three disk domain. Catalytic sites (heavy lines) and three escaping/reinjected pairs of trajectories are shown. Each pair is coded (circle, square, blank) to clearly identify it.

The disks are separated enough to permit a class of trajectories that never strike a disk; these trajectories never deviate from a straight-line path. When the disks are close enough to prevent this class of trajectories, it is known that the system has strong ergodic properties.<sup>7</sup> However, even when this is not the case (as in our system), this class has zero measure in the class of all trajectories, and the other trajectories sample the available phase space ergodically. This implies that there is an equilibrium color distribution of half black and half white, each half being distributed uniformly throughout the system.

### A. Color correlation function

We are interested in the rate of return to (color) equilibrium after the system is perturbed. Denoting the deviation of the black number from its equilibrium value by  $\delta \bar{n}_B = \bar{n}_B - \bar{n}_B^{\text{eq}}$ , Eq. (16) gives

$$\frac{d \delta \bar{n}_B}{dt} = k(\delta \bar{n}_W - \delta \bar{n}_B) = -2k \delta \bar{n}_B, \quad (17)$$

yielding a simple exponential decay with decay constant  $\gamma_r = 2k$ . In writing this equation we have used the fact that  $\delta \bar{n}_W = -\delta \bar{n}_B$ .

To probe this relaxation to equilibrium after a small perturbation, we invoke Onsager's regression hypothesis and shift our attention to fluctuations in the equilibrium system. Consequently, we define the autocorrelation function of the deviation of the number of black particles from its average value as

$$C(t) = \langle \delta \chi_B(t) \delta \chi_B(0) \rangle, \quad (18)$$

where  $\chi_B$  is the dynamical variable for the black species; i.e.,  $\chi_B = 1$  if the particle is black and zero if it is white. The angle brackets signify a time average over a long trajectory

$$\langle A(t)B(0) \rangle = \frac{1}{T} \int_0^T dt' A(t+t')B(t'). \quad (19)$$

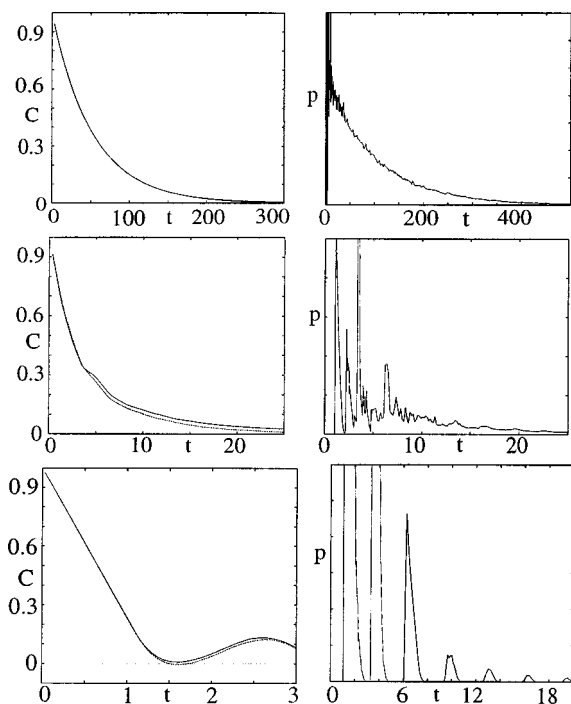


FIG. 12. The top left panel shows the correlation function for a catalytic site on disk one spanning the angular domain  $\theta \in [\pi/6 \pm 0.04]$ . Also shown is the correlation function obtained by sampling from the distribution alone (see text; these are indistinguishable on the scale of the figure). The middle left panel is for a catalytic site covering all of disk one. The solid line is the correlation function  $C(t)$  computed from the trajectory, while the dashed line is the correlation function  $C_D(t)$  obtained by sampling from the distribution alone. The bottom left panel is for a catalytic site covering all three disks. The corresponding panels on the right hand side show the distribution of times between color changes (ordinate in arbitrary units).

The deviation  $\delta\chi_B$  is defined as  $\delta\chi_B = \chi_B - \langle \chi_B \rangle$ . The times  $t'$  are chosen generically to provide a representative sample of the particle's behavior.

### B. Small catalytic domains

The exponential decay expected on the basis of the phenomenological law is borne out for a catalytic site with small measure. The left panels of Fig. 12 show plots of the black particle autocorrelation function versus time for various choices of the measure of the catalytic region. The microscopic basis for this agreement can be understood from the following considerations. For a catalytic site with small enough measure there are essentially no correlations between successive reactions since the trajectory is quickly randomized. The distribution of times between successive reactions follows the exponential (interarrival time) distribution of a Poisson process, except for a very short initial time period (Fig. 12, upper right panel). Given that the correlation function decays exponentially we can easily extract the decay constant  $\gamma_r$ . This value can be compared with the analog of a transition-state theory calculation of the rate constant for this process. The transition-state region may be defined as the phase space domain containing particles that will strike the catalytic site in a short time  $\Delta t$ . The time  $\Delta t$  should be sufficiently small that no more than one collision event with

TABLE II. Comparison of  $\gamma_r$  and  $\gamma_{TS}$  for catalytic sites of varying measures all centered at  $\theta = \pi/6$  on disk one.

$\varphi$	$\gamma_r$	$\gamma_{TS}$
0.014	0.0034	0.0034
0.04	0.0097	0.0097
0.10	0.023	0.024
0.20	0.044	0.049
0.40	0.08 (Ref.18)	0.097

the site occurs. The transition-state rate constant is then given by the probability density of being in the transition state region,

$$\gamma_{TS} = 2k_{TS} = 2 \frac{2\varphi a}{2\pi A}, \quad (20)$$

where  $2\varphi a$ , with  $\varphi$  being the angle subtended by the catalytic site, comes from Eq. (13), and

$$2\pi A = 2\pi \left( \frac{\sqrt{3}}{4} R^2 - \frac{1}{2} \pi a^2 \right), \quad (21)$$

is the total phase space volume in a single three-disk domain. Using the numerical values of  $R=3.11$  and  $a=1$  gives  $\gamma_{TS} = 0.243\varphi$ . Table II compares this ‘‘transition-state’’ rate constant with the rate constant obtained directly from the correlation function  $C(t)$ . As the measure of the catalytic site increases,  $\gamma_{TS}$  overestimates  $\gamma_r$  because of correlated recollisions with the catalytic site.

### C. Large catalytic domains

When the catalytic site has large measure, possibly extending over several disk surfaces, correlations between reactive events lead to a breakdown of the simple phenomenological picture of the reaction, and the decay of the correlation function  $C(t)$  is not exponential (middle and bottom left-hand plots of Fig. 12).

The distribution of times between successive reactions is, for the bottom two right-hand panels of Fig. 12, clearly not Poissonian (exponential). For these large catalytic sites trajectories are likely to change color often, either from one reinjection to the next or within the same reinjection. These collisions are too frequent for the trajectory to be randomized between color changes—there are correlations between successive color changes which introduce structure into the distribution of times between reactions. This structure is extremely pronounced in the bottom right panel of Fig. 12, where a color change and a collision event with a disk are synonymous. This structure and the severe breakdown of the phenomenological picture is the result of two time scales being nearly equal—the time scale for reaction (color change) and the time scale for randomization. It is the relative magnitudes of these two time scales which determines the validity of the assumptions implicit in a Poisson process description and hence in the phenomenological picture.

We test the importance of the time-ordered arrangement of color intervals on the correlation function by computing a new correlation function  $C_D(t)$  using only the distribution of times between successive reactions. A new ‘‘trajectory’’ is

constructed by sampling from this distribution. The resulting correlation functions are shown in Fig. 12. They are very similar to the full correlation functions  $C(t)$ , allowing us to conclude that the distribution function alone accounts for the shape of the correlation decay  $C(t)$ .

## VI. CONCLUSION

The three-disk system studied here is transiently chaotic. Trajectories near the underlying repeller of the system survive for a long time but ultimately escape. These trajectories constitute the microscopic dynamics that give rise to the phenomenological (and observed) exponential decay of particle density in the system. Nevertheless, for the reactive system, the colored exponential decay constants display a dependence on the location of the catalytic site. This dependence is linked to both the underlying repeller and the colored Kolmogorov–Sinai entropy. More specifically, our results indicate that Pesin’s theorem cannot be simply extended to the reactive case as defined in this study. The relationship between the escape rate and the Kolmogorov–Sinai entropy is opposite to that predicted by a simple extension of Pesin’s theorem. Our results show that new phenomena arise when classes of trajectories labeled by their reaction history are distinguished.

For the periodic lattice of scatterers with an array of catalytic sites, the microscopic criterion for the validity of the mass-action rate law is that the “interarrival” reaction times be Poissonian, implying that the trajectory is randomized between reactions. A sufficient condition for this is that the catalytic sites have small measure. The relative time scales of reaction and randomization determine whether or not the phenomenological picture is obeyed. This breakdown of mass-action kinetics has implications for the description

of reaction kinetics in confined geometries or situations where reactions are fast relative to other nonreactive processes in the system.

While the systems studied here are over-simplified models of real reactive dynamics they do capture some essential features of such systems and allow a detailed examination of the microscopic basis of chemical rate laws. The modeling of chemical reactions through open dynamical systems introduces new and interesting questions on extensions of chaotic measures, such as the Kolmogorov–Sinai entropy, to reactive dynamics.

- <sup>1</sup>N. DeLeon and B. J. Berne, Chem. Phys. Lett. **93**, 162 (1982); **93**, 169 (1982); J. Chem. Phys. **75**, 3495 (1981).
- <sup>2</sup>Y. Elskens and R. Kapral, J. Stat. Phys. **38**, 1027 (1985).
- <sup>3</sup>P. Gaspard and R. Klages, Chaos **8**, 409 (1998).
- <sup>4</sup>Y. Elskens, H. L. Frisch, and G. Nocolis, J. Stat. Phys. **33**, 317 (1983).
- <sup>5</sup>P. Gaspard and S. A. Rice, J. Chem. Phys. **90**, 2225 (1989).
- <sup>6</sup>P. Gaspard and G. Nocolis, Phys. Rev. Lett. **65**, 1693 (1990).
- <sup>7</sup>J. Machta and R. Zwanzig, Phys. Rev. Lett. **50**, 1959 (1983).
- <sup>8</sup>H. van Beijeren and J. R. Dorfman, Phys. Rev. Lett. **74**, 4412 (1995).
- <sup>9</sup>J. Machta and B. Reinhold, J. Stat. Phys. **42**, 949 (1986).
- <sup>10</sup>M. H. Ernst, J. R. Dorfman, R. Nix, and D. Jacobs, Phys. Rev. Lett. **74**, 4416 (1995).
- <sup>11</sup>J. Machta and S. M. Moore, Phys. Rev. A **32**, 3164 (1985).
- <sup>12</sup>H. van Beijeren and M. H. Ernst, J. Stat. Phys. **70**, 793 (1993).
- <sup>13</sup>H. Spohn, Rev. Mod. Phys. **53**, 569 (1980).
- <sup>14</sup>H. van Beijeren, Rev. Mod. Phys. **54**, 195 (1982).
- <sup>15</sup>C. Beck and F. Schlögl, *Thermodynamics of Chaotic Systems* (Cambridge University Press, Cambridge, 1993).
- <sup>16</sup>J. R. Dorfman and P. Gaspard, Phys. Rev. E **51**, 28 (1995).
- <sup>17</sup>It should be noted that the escape rate data has been scaled by the average intercollision distance of  $\langle d \rangle = 1.308$  in order to make it comparable with the entropy data.
- <sup>18</sup>The correlation function  $C(t)$  deviates from exponential decay at this catalytic site size. The value reported here is the best fit to an exponential function.